Discover Oncology

Research

Leveraging multiple cell-death patterns based on machine learning to decipher the prognosis, immune, and immune therapeutic response of soft tissue sarcoma

Binfeng Liu[1,2,3] · Shasha He[4] · Chenbei Li[1,2,3] · Zijian Xiong[1,2,3] · Zhaoqi Li[1,2,3] · Chengyao Feng[1,2,3] · Hua Wang[1,2,3] · Chao Tu[1,2,3,5,6] · Zhihong Li[1,2,3,5,6]

Received: 4 January 2025 / Accepted: 6 May 2025
Published online: 25 May 2025

Abstract

Soft tissue sarcomas (STS) imposes a substantial healthcare burden on society. The progression of these tumors is significantly influenced by diverse modes of programmed cell death (PCD), which can serve as valuable indicators for assessing prognosis and immune therapeutic response in STS. Nonetheless, the precise role of multiple cell death patterns in STS is yet to be clarified. We employed 96 machine-learning algorithm combination frameworks to identify novel cell death-related signatures (CDSigs) with the highest mean c-index, indicating their excellence. The independence test and comparison with previously published models further confirmed the stability and quality of these signatures for survival prediction in STS. The nomogram, comprising the cell death score (CDS) and clinical features, exhibited excellent predictive performance. Additionally, the CDSigs revealed associations with immune checkpoint genes and the immune microenvironment in STS. Furthermore, the results demonstrated that patients with lower CDS had the potential for greater benefit from immune therapeutic responses compared to those with higher CDS. Moreover, STS patients with low-risk scores exhibited heightened sensitivity to doxorubicin, axitinib, cisplatin, and camptothecin. Finally, the RT-qPCR results underscored significant differences in expression levels of several CDSigs genes between STS and normal cells. Overall, we comprehensively analyzed the multiple PCD in STS and established a novel CDSig for STS patients. This novel CDSig holds great promise in deciphering the prognosis, immune, and immune therapeutic response of STS.

Keywords Soft tissue sarcoma · Programmed cell death · Immune therapeutic response · Prognosis

Binfeng Liu and Shasha He have contributed equally to this work and share the first authorship.

Supplementary Information The online version contains supplementary material available at https://doi.org/10.1007/s12672-025-02587-z.

✉ Chao Tu, tuchao@csu.edu.cn; ✉ Zhihong Li, lizhihong@csu.edu.cn | [1]Department of Orthopaedics, The Second Xiangya Hospital, Central South University, Changsha 410011, Hunan, China. [2]Hunan Key Laboratory of Tumor Models and Individualized Medicine, The Second Xiangya Hospital of Central South University, Changsha 410011, Hunan, China. [3]Hunan Engineering Research Center of AI Medical Equipment, The Second Xiangya Hospital of Central South University, Changsha 410011, Hunan, China. [4]Department of Oncology, The Second Xiangya Hospital, Central South University, Changsha, Hunan, People's Republic of China. [5]Shenzhen Research Institute of Central South University, Guangdong 518063, China. [6]National Clinical Research Center for Mental Disorders, and National Center for Mental Disorders, The Second Xiangya Hospital of Central South University, Changsha, China.

Abbreviations

STS	Soft tissue sarcomas
ACD	Accidental cell death
PCD	Programmed cell death
TCGA	The cancer genome atlas
TARGET	The therapeutically applicable research to generate effective treatments
GEO	Gene expression omnibus
GTEx	Genotype-tissue expression
DEG	Differentially expressed genes
CNV	Copy number variation
CDSig	Cell death-related signatures
RSF	Random survival forest
Enet	Elastic net
plsRcox	Cox partial least squares regression
SuperPC	Supervised principal component
GBM	Generalized boosted regression modeling
Survival-SVM	Survival support vector machine
CDS	Cell death scores
AUC	Area under the curve
ROC	Receiver operating characteristic
DCA	Decision curve analysis
SNV	Single nucleotide variation
ssGSEA	Single-sample gene set enrichment analysis
TIDE	Tumor immune dysfunction and exclusion
Submap	Subnetwork mappings in alignment of pathways
FBS	Fetal bovine serum
DFS	Disease-free survival

1 Introduction

Soft tissue sarcomas (STS) encompass a rare and diverse group of malignant tumors that arise primarily from the mesoderm, with some originating from the neuroectoderm. These tumors differentiate into non-epithelial extraskeletal tissues, including muscle, fat, mucus, mesothelium, blood vessels, and lymphatic vessels [1, 2]. Currently, there are more than 50 subtypes of STS, found in 19 different types of tissues, and they can occur in various regions of the body [3, 4]. STS constitutes approximately 1% of malignant tumors in adults, with an annual incidence of 3,300 cases in the United Kingdom and 10,000 cases in the United States [5]. While STS can manifest at any age, its incidence increases with age, and the average mortality rate across all age groups is around 50% [6]. Currently, surgery is the standard treatment for localized STS and often requires preoperative radiation therapy and interventional procedures to create conditions that facilitate the achievement of a safe surgical margin. Additionally, chemotherapy is administered postoperatively, depending on the specific patient's characteristics [7, 8]. However, STS is prone to recurrence and distant metastasis, with 16% of patients already showing distant metastasis at the time of diagnosis. Despite initial treatment, 10–30% of patients experience relapse, and 30–40% develop distant metastasis [9]. The recurrence and distant metastasis of STS present significant challenges and impose a substantial health burden. Given the current treatment challenges, there is an urgent need to explore effective models that can improve prognosis and enable precise treatment of STS.

Cell death occurs through two primary mechanisms: accidental cell death (ACD) and programmed cell death (PCD), each triggered by distinct mechanisms. ACD is an uncontrollable biological process, while PCD is a genetically determined form of active cell death. PCD encompasses various modes, including apoptosis, necroptosis, ferroptosis, pyroptosis, netotic cell death, entotic cell death, lysosome-dependent cell death, parthanatos, autophagy-dependent cell death, oxeiptosis, alkaliptosis, all closely linked to homeostasis and disease [10]. Activation of diverse cell death pathways, either directly or indirectly, to hinder tumor proliferation, invasion, and metastasis holds promise in cancer therapy. However, excessive cell death can create an inflammation-associated immunosuppressive microenvironment, promoting cancer progression and recurrence [11]. For decades, PCD has been established as a fundamental player in the development

and metastasis of malignant tumors. Overcoming various forms of cell death is essential for hindering the progression of malignant tumor cells [12]. With advancements in gene chip and sequencing technology, an increasing number of studies focus on constructing cancer prognostic signatures based on the expression of programmed death-related genes, yielding encouraging results [13]. For example, Liu et al. demonstrated that the immunogenic cell death-related model could predict the prognosis and tumor immunity microenvironment of osteosarcoma [14]. While numerous cell death-associated features of STS have been identified, most studies have primarily focused on the significance of individual cell death pathways in cancer prognosis. Therefore, it is crucial to emphasize a prognosis signature for STS based on a comprehensive summary of PCD.

In this paper, we aim to collect a comprehensive set of PCD-related genes from existing literature and relevant databases. By employing bioinformatics methods and machine learning, we developed a novel index specific to STS. Within this framework, we investigated the impact of this index on the progression and prognosis of STS. We examined its intricate relationships with tumor immune at multiple levels and its potential integration into immune therapeutic strategies, further enhancing its clinical relevance for predicting the prognosis of STS patients. Additionally, we identified potential drugs associated with this index, laying the groundwork for further exploration of molecular mechanisms and medical interventions.

2 Materials and methods

2.1 Data collection

In this study, we acquired a comprehensive set of 1078 PCD-related genes from prior research, encompassing key regulatory genes across the identified 12 PCD patterns [15]. The sarcoma dataset, comprising transcriptome data and corresponding clinical information, was sourced from multiple databases, namely, The Cancer Genome Atlas (TCGA, https://portal.gdc.cancer.gov), The Therapeutically Applicable Research to Generate Effective Treatments (TARGET, https://ocg.cancer.gov/programs/target), and Gene Expression Omnibus (GEO, http://www.ncbi.nlm.nih.gov/geo). Correspondingly, the detailed clinical information of the patients in the cohort mentioned above is listed in Table S1-S4. Four datasets, totaling 969 patient samples, were downloaded, comprising the TCGA dataset (259 samples), the TARGET dataset (88 samples), the GSE21050 dataset (310 samples), and the GSE71118 dataset (312 samples), providing a comprehensive representation of sarcoma data. Furthermore, normal tissue sequencing samples from the Genotype-Tissue Expression (GTEx, https://www.gtexportal.org/home/) database served as controls for subsequent differential gene analysis, involving a total of 912 connective tissue, skeletal muscle, and subcutaneous fat tissue samples. Subsequently, probe names were converted to gene symbols, and the raw transcriptome data underwent normalization and log2 transformation. The probes were mapped using "AnnoProbe" R package.

2.2 Screening differential expressed PCD-related prognostic genes.

Utilizing transcriptome data previously acquired from sarcoma and normal control tissues, we conducted a differential expression analysis using the"edgeR"package to identify differentially expressed genes (DEGs) between the two cohorts. The screening criteria we applied were $P < 0.05$ and $|\log2\ FC| > 1$. To confirm the discriminative capacity of the DEGs between tumor and normal control tissues, we employed principal component analysis (PCA) and uniform manifold approximation and projection (UMAP) analyses. Furthermore, we used univariate Cox regression analysis to identify prognostic-related genes. We then explored somatic mutation information for the differentially expressed prognostic genes related to PCD in STS using the"maftools"package, which presented the top 20 mutation rates in a waterfall diagram. Additionally, we depicted the copy number variation (CNV) values of the differentially expressed prognostic genes related to PCD in histograms, categorizing them into three situations: CNV gain, CNV loss, and no CNV.

2.3 Construction of cell death-related signatures (CDSig)

Based on previous reference literature, we constructed a novel CDSig by combining multiple algorithms, including Random Survival Forest (RSF), Elastic Net (Enet), Lasso, Ridge, Stepwise Cox, Cox Boost, Cox Partial Least Squares Regression (plsRcox), Supervised Principal Component (SuperPC), Generalized Boosted Regression Modeling (GBM), and Survival Support Vector Machine (survival-SVM) [16]. We initially applied the first machine learning algorithm for feature

selection to identify gene variables used for model development. Subsequently, the second machine learning algorithm was employed to construct the predictive model based on the selected gene variables, which was then validated in an independent validation cohort. The TCGA-STS dataset served as the training set, while the remaining three independent cohorts were designated as the testing set. The predictive feature's C-index value in each cohort was then calculated based on the combination of the aforementioned machine learning algorithms, resulting in an average C-index. Consequently, the prognostic feature with the highest average C-index was identified as the optimal CDSig. Subsequently, individual Cell Death Scores (CDS) were calculated for each subject based on the optimal CDSig. The sarcoma patient cohort was then divided into low-CDS and high-CDS groups according to the median CDS. Kaplan–Meier analysis, utilizing the "survival" and "survminer" packages, was conducted to explore the relationship between overall survival status and CDS in sarcoma patients.

Furthermore, the prognostic assessment value of CDSig for sarcoma patients was systematically evaluated. The accuracy of prognostic assessment by CDSig was determined through the Area Under the Curve (AUC) of the Receiver Operating Characteristic (ROC) curve drewed by the"timeROC"R package. The c-index was employed for a comprehensive evaluation of all clinical features in predicting prognosis for sarcoma, further validating the predictive performance of CDSig. Simultaneously, a calibration curve was used to assess the agreement between the predicted survival rate by CDSig and the actual survival rate of the sarcoma cohort. Additionally, a systematic search of prognostic signatures for STS was conducted on PubMed to compare their predictive performance with the novel CDSig.

2.4 Cox regression analysis and nomogram development

To assess the independence of the newly developed CDSig, we conducted both univariate and multivariate Cox regression analyses based on patients'overall survival time, considering CDSig along with other clinical factors. Simultaneously, gender, age, and metastatic status (Primary metastasis or metastasis at follow-up) were combined with CDSig to construct a prognostic nomogram using the"regplot"and"rms"packages. Subsequently, we used the"caret"and"rmda"R packages to create a calibration plot and perform Decision Curve Analysis (DCA) to evaluate the effectiveness of the nomogram. ROC analysis was carried out using the"timeROC"R package.

2.5 Functional enrichment analysis

To explore the unique biological functions associated with the low- and high-CDSig groups, we conducted functional enrichment analysis using the R package"clusterProfiler"to identify biological pathways. We employed a network analysis to illustrate the regulatory connections and prognostic significance of CDSig genes. Additionally, we evaluated differences in intratumor heterogeneity, proliferation, and TGF-beta response scores between STS cohorts characterized by varying CDS. Briefly, we obtained the intratumor heterogeneity, proliferation, and TGF-β response scores for each TCGA STS patient from prior studies [17]. The STS cohort was then stratified into distinct groups based on their CDS scores. Finally, we compared the differences in intratumor heterogeneity, proliferation, and TGF-β response scores across the CDS groups and visualized these differences using violin plots, which illustrate the distribution and variability of each score within the CDS-defined groups.

2.6 Immune infiltration analysis

The tumor immune microenvironment plays a crucial role in tumor progression and significantly influences patient prognosis. Therefore, we conducted a comprehensive analysis to explore the association between the newly developed CDSig and immune infiltration. We used the ESTIMATE algorithm to infer and score the proportions of stromal and immune cells [18]. Additionally, we employed the CIBERSORT algorithm to assess the relative infiltration levels of 22 immune cell types in STS cohorts [19]. We also investigated variations in expression levels of important immune checkpoints among patients with different CDS groups and explored the correlation between CDS and immune scores, the extent of immune cell infiltration, and expression levels of key immune checkpoints. To assess differences between distinct CDSig groups, we performed comparative analyses of Leukocyte Fraction, Lymphocyte Infiltration Signature score, and single nucleotide variation (SNV) neoantigens [20]. Furthermore, we examined disparities in immune-related genes between the two groups, considering expression, mutation, amplification, deletion, and methylation levels. Finally, we used the Single-Sample Gene Set Enrichment Analysis (ssGSEA) algorithm to quantify changes in immune cell-related functions in STS [21].

2.7 Immune therapeutic response prediction

To predict immune therapeutic response, we employed the Tumor Immune Dysfunction and Exclusion (TIDE) algorithm to assess the TIDE score for each patient, where"true"indicated a more favorable immunotherapy response, and"false"denoted a poorer response. Simultaneously, the Subnetwork Mappings in Alignment of Pathways (Submap) approach was utilized to assess immunotherapy responses (anti-PD-1 and anti-CTLA-4), considering a p-value less than 0.05 indicative of sensitivity to immunotherapy. Furthermore, we validated the predictive performance for immunotherapy using the IMvigor210 and Liu David datasets. Additionally, we delved into the relationship between survival time, immunotherapy effects, and CDS.

2.8 Cell culture

For the experimental validation, we selected the human skin fibroblast cell line (HSF) and sarcoma cell lines, namely SW872, SYO-1, and 005R. The origins of these cells align with the information provided in previous research reports [22–24]. Following the described methodology, the cells were cultured in DMEM supplemented with 10% fetal bovine serum (FBS) and 1% penicillin–streptomycin solution. Additionally, all cell cultures were maintained in a 37 °C incubator with 5% CO2.

2.9 RNA extraction and real-time quantitative PCR(RT-qPCR).

Following the procedures described in our previous publication, we performed RNA extraction and RT-qPCR [25]. GAPDH was used as the internal control for the target gene, and the expression level of the target gene was calculated using the $2^{-\Delta\Delta Ct}$ method. The primer sequences utilized in this study are available in Table S5.

2.10 Statistical analysis

All statistical analyses were performed using R software (version 4.1.0) and GraphPad Prism (version 9.0.0). Differential analysis was conducted using the R package "limma." Kaplan–Meier plots were used to illustrate survival curves and differences in survival times were evaluated using the log-rank test. Student's t-test was used to compare continuous variables between two groups, while the Wilcoxon test was used for non-normally distributed variables. For comparisons involving multiple groups, One-way ANOVA analysis was employed. Pearson's correlation test was utilized to determine interactions between variables. When $P < 0.05$, the difference was considered statistically significant.

3 Results

3.1 Identification of differentially expressed PCD-related genes in STS

The study's flowchart is presented in Fig. 1. Through a comparison of STS tissues with normal control tissues, a total of 439 DEGs associated with PCD were identified. The corresponding expression levels of these DEGs are depicted in the heat map shown in Fig. 2A. Additionally, the use of PCA and Umap analysis demonstrated the effectiveness of these DEGs in differentiating between STS and normal control tissues (Fig. 2B, C). Furthermore, a functional enrichment analysis based on these DEGs revealed their significant involvement in various biological pathways. Notably, both upregulated and downregulated DEGs were found to be enriched in programmed death regulatory pathways, including apoptotic signaling, regulation of apoptotic signaling, and regulation of autophagy (Fig. 2D, E). Utilizing Cox regression analysis, a subset of 84 DEGs associated with prognosis was identified from the pool of DEGs related to PCD (Fig. 2F). Moreover, an evaluation of mutation frequencies was conducted for these prognostic DEGs within the STS patient cohort, consisting of 57 individuals. The results indicated that 26 patients (45.61%) exhibited mutations, with the top 20 frequently mutated genes illustrated. Among these genes, PLCG1 had the highest mutation frequency (7%), while the others ranged from 2 to 5% (Fig. 2G, H). Lastly, an analysis of CNV status unveiled frequent

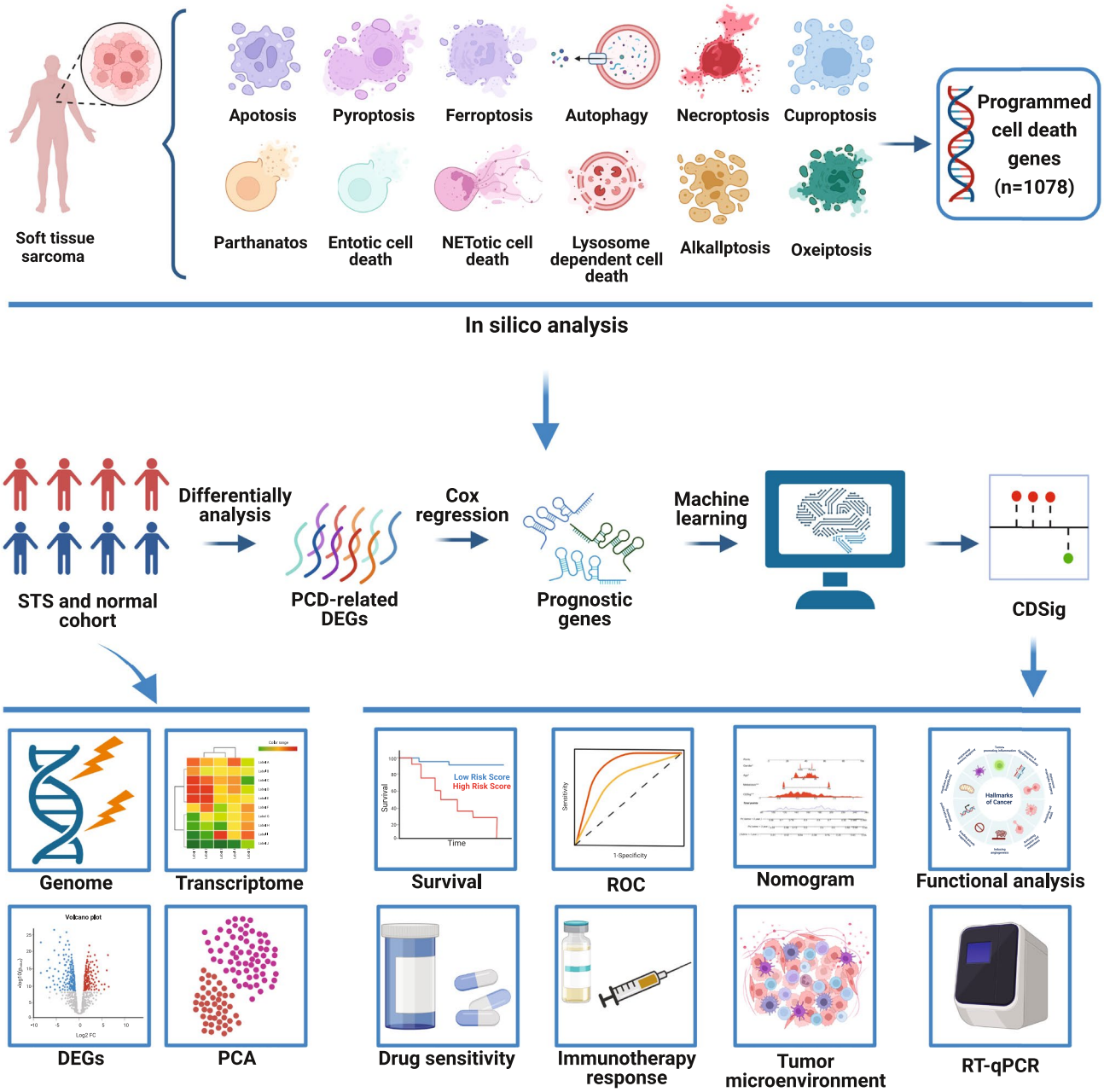

Fig. 1 Flowchart for comprehensive analysis of diverse cell death patterns in STS

alterations in DEGs linked to prognosis. Notably, FOXO1 displayed the most extensive CNV loss, while DAP, GSS, NFS1, PLCG1, and others exhibited substantial copy number amplifications (Fig. 2I).

3.2 Construction of the novel CDSig

To develop a CDSig with optimal effectiveness, we integrated 84 prognosis DEGs into 96 program frameworks generated by 10 machine learning algorithms. Model development involved tenfold cross-validation. Among these models, the one based on the RSF and SuperPC algorithm demonstrated the highest average C-index value, indicating the most optimal CDSig (Fig. 3A). The error bar plot in Fig. 3B depicts the RSF analysis process. This CDSig consists of 25 genes with the greatest significance, and their respective importance is illustrated in Fig. 3C. Furthermore, the impact of these genes on the prognosis of STS patients is visualized in Figure S1 and Figure S2. Since the GSE21050 and GSE71118 datasets do not

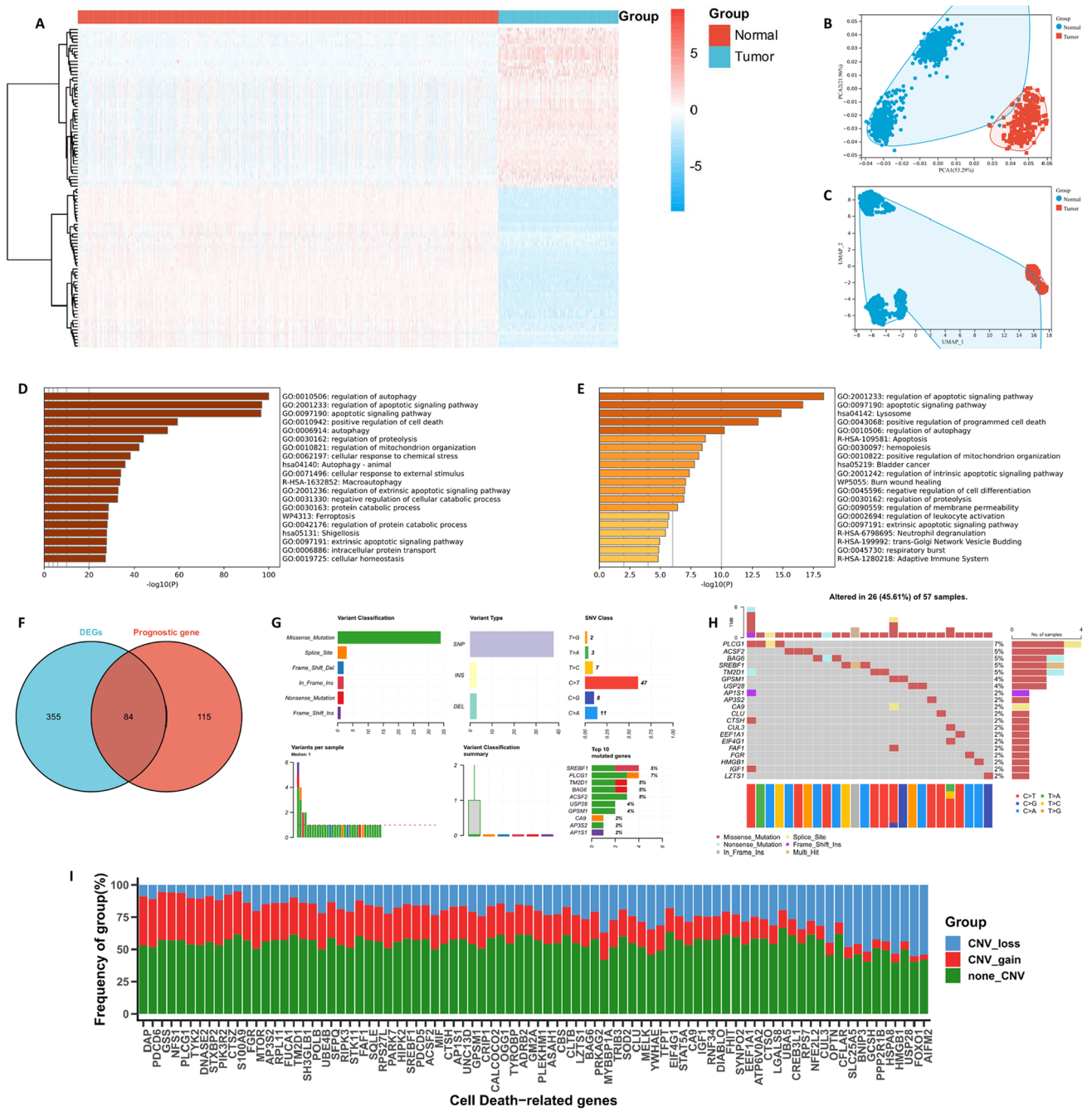

Fig. 2 Exploring programmed cell death (PCD)-related genes in STS based on the TCGA database. **A** Heatmap of the PCD-related DEGs between STS and normal tissues. **B**, **C** PCA and Umap analysis of the PCD-related DEGs in STS and normal tissues. **D**, **E**. GO enrichment analyses based on the upregulated and downregulated DEGs. **F** Venn diagram of PCD-related DEGs and the PCD-related genes associated with the prognosis of STS. **G**, **H**. An oncoplot and waterfall plot of these 84 prognostic DEGs in the STS cohort. **I** CNV values of these 84 prognostic DEGs in the STS cohort. *DEGs* differentially expressed genes; *CNV* copy number variation

contain complete clinical information, we subsequently conducted a further prognostic analysis based on the TCGA and TARGET cohorts. We observed that STS patients with high CDS had considerably poorer survival times in both the TCGA and TARGET cohorts (Fig. 3D). Consistently, survival analysis was performed in the chemotherapy-treated TCGA cohort to evaluate the predictive potential of CDS, and the results showed that patients with low CDS had a better prognosis among STS patients who had received chemotherapy (Figure S3). However, consistent results were not obtained in GSE21050 and GSE71118, potentially due to differences in sequencing platforms or the survival data in these two datasets representing Disease-Free Survival (DFS). Moreover, the Area Under the Curve (AUC) values of the 1-year, 3-year, and

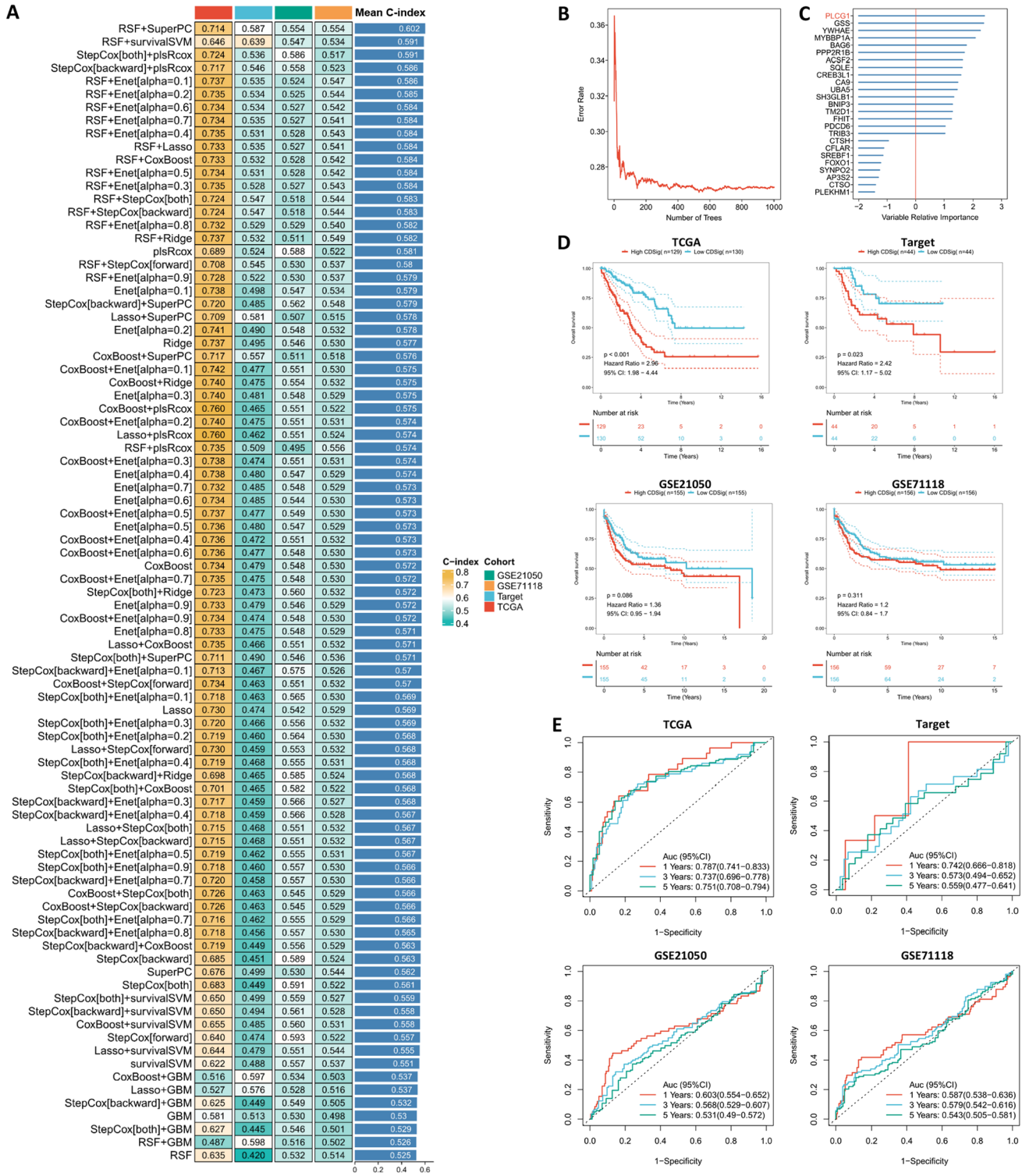

Fig. 3 Construction of a prognostic CDSig for STS patients. **A** The C-index of 96 machine learning algorithms in TCGA, TARGET, GSE21250, and GSE71118 cohorts. Training set: TCGA-STS dataset; Testing set: TARGET, GSE71118, and GSE21050 dataset. **B** The error bar of the RSF analysis process (TCGA cohort). **C** The exhibition of the 25 most valuable signature genes in STS (TCGA cohort). **D** Kaplan–Meier survival analysis between the high- and low-CDSig risk groups in TCGA, TARGET, GSE21250, and GSE71118 cohorts. **E** The Time-dependent ROC curves of 1-year, 3-year, and 5-year OS in TCGA, TARGET, GSE21250, and GSE71118 cohorts. CDSig: cell death-related signatures

5-year ROC curves in TCGA were 0.787, 0.737, and 0.751, respectively. Nevertheless, the AUC values in the ROC curves for the other three datasets were relatively unsatisfactory (Fig. 3E). Therefore, a comprehensive evaluation of the prognostic performance of the novel CDSig is warranted.

3.3 Prognostic value of the CDSig

Subsequently, we assessed the C-index value of the CDSig in both the TCGA and TARGET cohorts in comparison to other clinical features. The findings revealed that CDSig exhibited the most robust prognostic performance in the TCGA cohort, ranking second only to metastatic status in the TARGET cohort (Fig. 4A). Furthermore, the calibration curve provided additional insight into the predictive accuracy of the novel CDSig (Fig. 4B). Simultaneously, univariate Cox regression analysis demonstrated the association between CDSig and prognosis in both TCGA and TARGET cohorts (Fig. 4C). Similarly, multivariate Cox regression analysis confirmed CDSig as an independent predictor for STS (Fig. 4D). With the advancements in next-generation sequencing technology and big data mining, predictive signatures based on gene expression have been extensively explored. To comprehensively compare the performance of CDSig with other signatures, we systematically gathered previously published signatures. In total, 33 signatures were included in this study, the corresponding coefficients and the corresponding references are provided in the supplementary table (Table S6). These signatures were closely associated with various biological features, encompassing immunotherapy response, autophagy, ferroptosis, apoptosis, necroptosis, cuproptosis, etc. Remarkably, the C-index of CDSig signatures in the TCGA, TARGET, GSE21050, and GSE71118 datasets surpassed the majority of previous signatures (Fig. 4E).

3.4 Development and evaluation of the nomogram

In the realm of clinical decision-making, the consideration of clinical characteristics is crucial as it greatly influences patient prognosis. To enhance the accuracy of survival predictions, we developed a nomogram that integrates the CDSig with other essential clinical characteristics based on the TCGA cohort. Displayed in Fig. 5A, this nomogram incorporates Gender, Age, Metastasis status, and CDSig to assess the 1-, 3-, and 5-year survival probabilities for STS patients. Based on this nomogram, clinicians can estimate the 1-, 3-, and 5-year survival probabilities of STS patients according to their clinical characteristics. To further validate the reliability of this nomogram for prognostic assessment, we generated the calibration curve, AUC, and DCA curve. The calibration curve vividly illustrates the alignment between predicted and actual survival rates (Fig. 5B). Moreover, the AUC value of this nomogram surpasses that of other factors, highlighting its superior predictive performance (Fig. 5C). Additionally, the DCA reveals that the nomogram can provide enhanced clinical benefits in guiding the decision-making process for STS patients (Fig. 5D). In summary, the nomogram emerges as a valuable tool, providing each patient with a precise survival probability and thereby assisting clinicians in informed decision-making and the realization of personalized medicine.

3.5 Potential biological process related to the CDSig

Functional enrichment analysis was further applied to explore differences in biological processes between subgroups classified by CDS. In Fig. 6A and B, the top 20 biological processes enriched in the high CDS group and low CDS group are presented, respectively. Remarkably, the high CDS group is notably associated with processes related to development and cell adhesion, including growth, embryonic morphogenesis, and cell–cell differentiation. Conversely, individuals with low CDS are correlated with immune-related pathways such as the chemokine-mediated signaling pathway, immune effector processes, and negative regulation of the immune system process, indicating a potential connection between low CDS and enhanced immune-related functions. Additionally, Fig. 6C illustrates the correlation and prognostic relationships among CDSig genes, underscoring their close interrelation. Interestingly, the high-risk group exhibits higher intratumor heterogeneity, proliferation, and TGF-beta response scores compared to the low-risk group (Fig. 6D–F), suggesting a potential association between elevated CDS and malignant biological behaviors.

3.6 The novel CDSig exhibits substantial immune-related characteristics.

Furthermore, we conducted an analysis to discern variations in immune features between the two CDSig groups. As illustrated in Fig. 7A, the outcomes reveal enhancements in Stromal score, ESTIMATE score, immune score, the infiltration abundance of Macrophages M1, T cell CD8, Dendritic cells resting, and Mast cell resting, alongside increased expression of

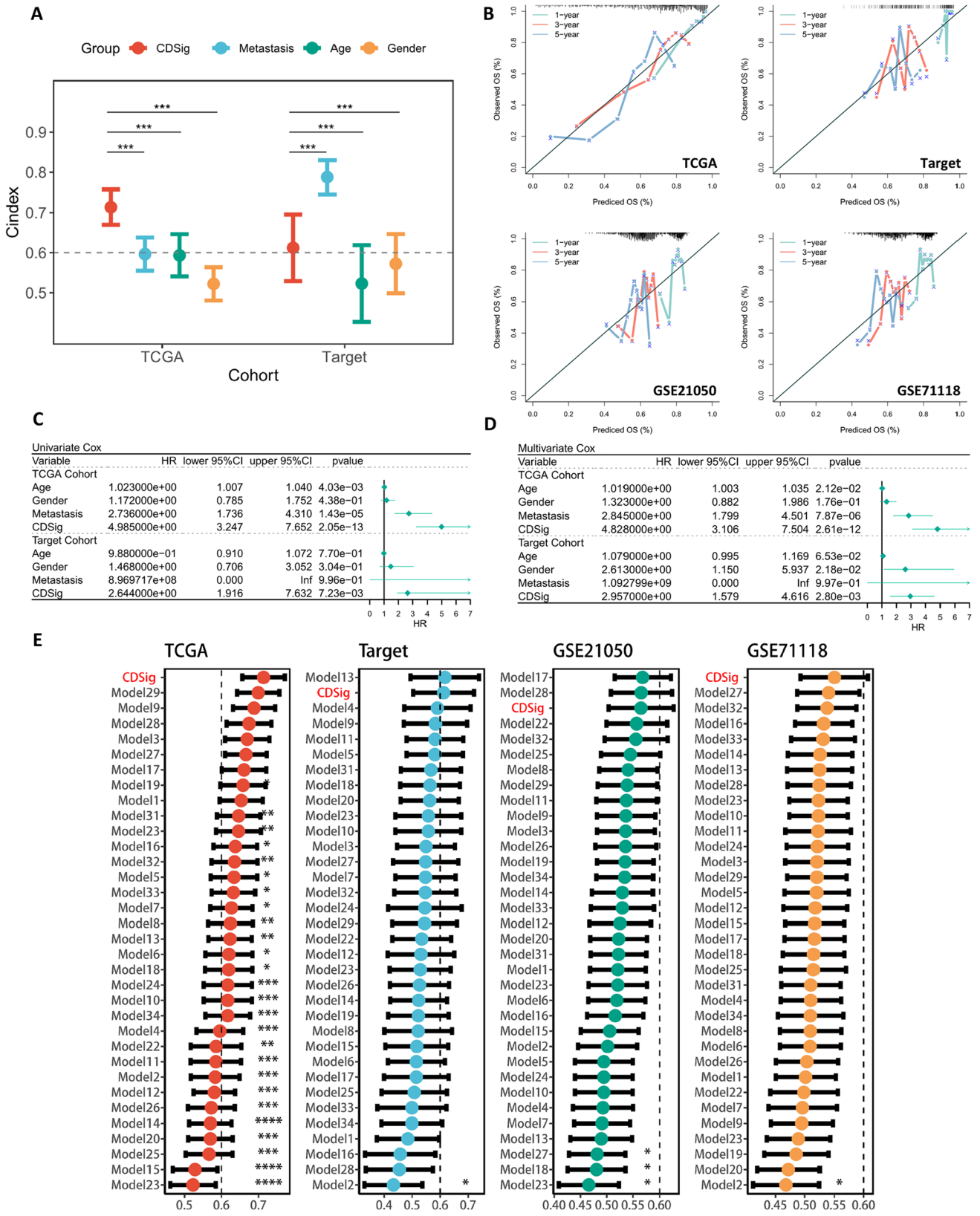

Fig. 4 The prognostic value of the novel CDSig in STS patients. **A** The prognosis prediction performance of CDSig compared to common clinical features and molecular variables in TCGA and TARGET cohorts. **B** The calibration curve of CDSig in TCGA, TARGET, GSE21250, and GSE71118 cohorts. **C** Univariate analysis for the clinicopathologic characteristics and CDS in TCGA and TARGET cohort. **D** Multivariate analysis for the clinicopathologic characteristics and CDS in TCGA and TARGET cohort. **E** The C-indexes of CDSig and other published signatures in TCGA, TARGET, GSE21250, and GSE71118 cohorts. CDSig: cell death-related signatures; OS: Overall survival

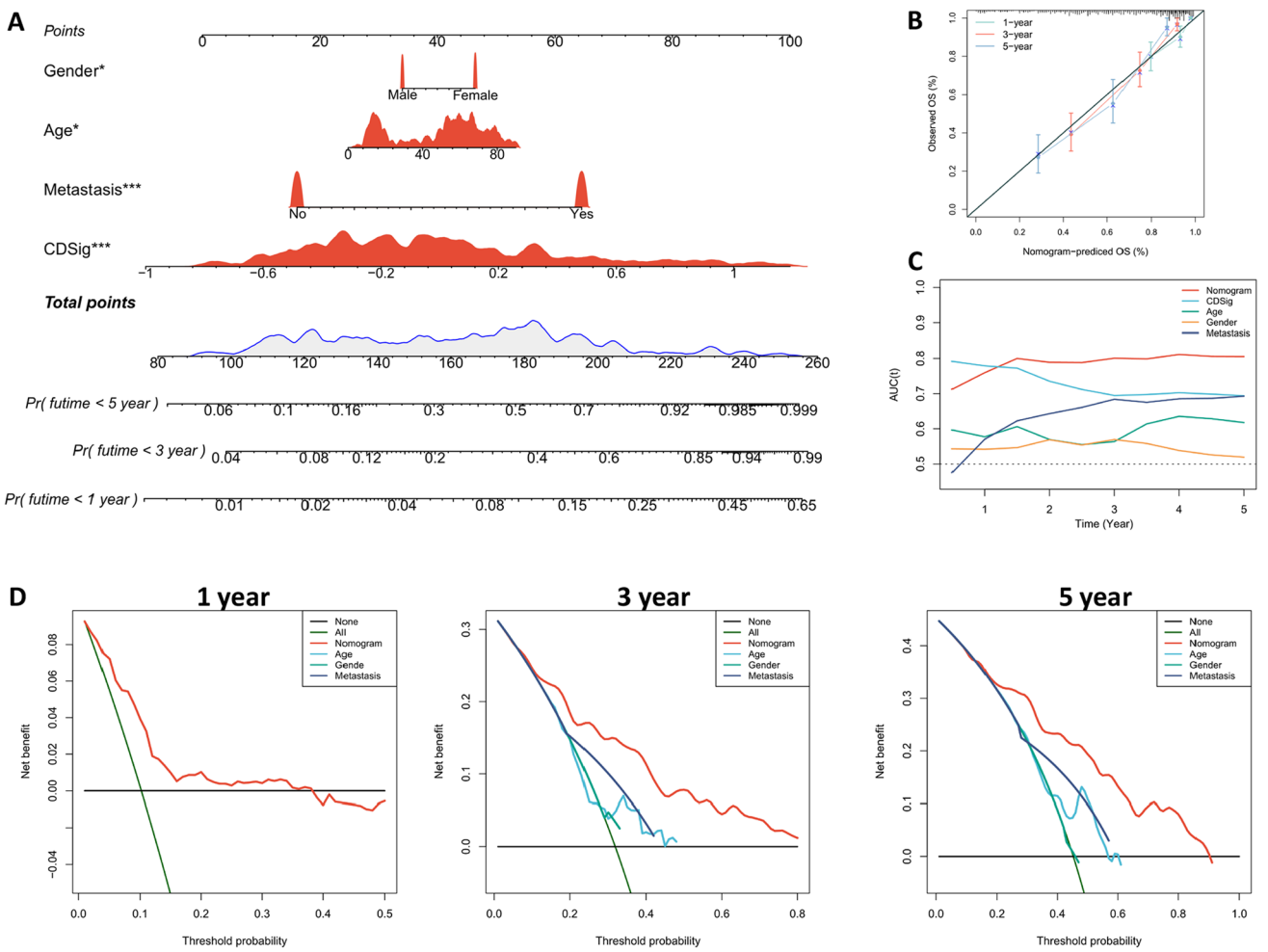

Fig. 5 Establishment and assessment of the nomogram survival model based on the TCGA database. **A** A nomogram was established to predict the prognostic of STS patients. **B** Calibration plots showing the probability of 1-, 3-, and 5-year overall survival in the TCGA cohort. **C** The AUC of the Nomogram and other characteristics in STS. **D** Decision curve analysis (DCA) of a nomogram predicting 1-, 3-, and 5-year overall survival. CDSig: cell death-related signatures

CTLA-4 and PD-1 in the low CDSig group. Conversely, the tumor purity score, infiltrated Macrophages M0, NK cell resting, Mast cells, and the expression of PD-L1 and PD-L2 were reduced in the low CDSig group. Concurrently, a substantial correlation was observed between CDSig and Stromal score, ESTIMATE score, immune score, tumor purity score, infiltrated Macrophages M0, NK cell resting, plasma cells, Macrophages M1, T cell CD8, Dendritic cells resting, Mast cell resting, and the expression of TIM3, LAG3, and PD-1 (Fig. 7B). Remarkably, ssGSEA indicated an activated immune function in the low CDSig group (Figure S4A). Additionally, patients with lower CDS exhibited an upregulated level of leukocyte fraction, Lymphocyte Infiltration Signature score, and SNV Neoantigens (Fig. 7C–E). Furthermore, we observed significant differences in the expression, mutation, amplification, deletion, and methylation levels of most immune-related molecules between distinct CDSig groups (Figure S4B-E).

3.7 The immunotherapy response and drug sensitivity predicting the efficiency of CDSig

Building upon the previous findings, we hypothesized that a low CDS may correlate with a more favorable response to immunotherapy. Therefore, we investigated the association between CDSig and the response to immunotherapy. As anticipated, individuals with low CDSig scores in both the TCGA and TARGET cohorts exhibited a greater inclination toward responding to immunotherapy (Fig. 8A: TCGA cohort; Fig. 8C: TARGET cohort). Similarly, patients in the low CDSig group were more likely to respond to anti-CTLA-4 and anti-PD1 immunotherapy (Fig. 8B: TCGA cohort; Fig. 8D: TARGET cohort). These findings collectively indicate that patients with low CDS may derive increased benefits from

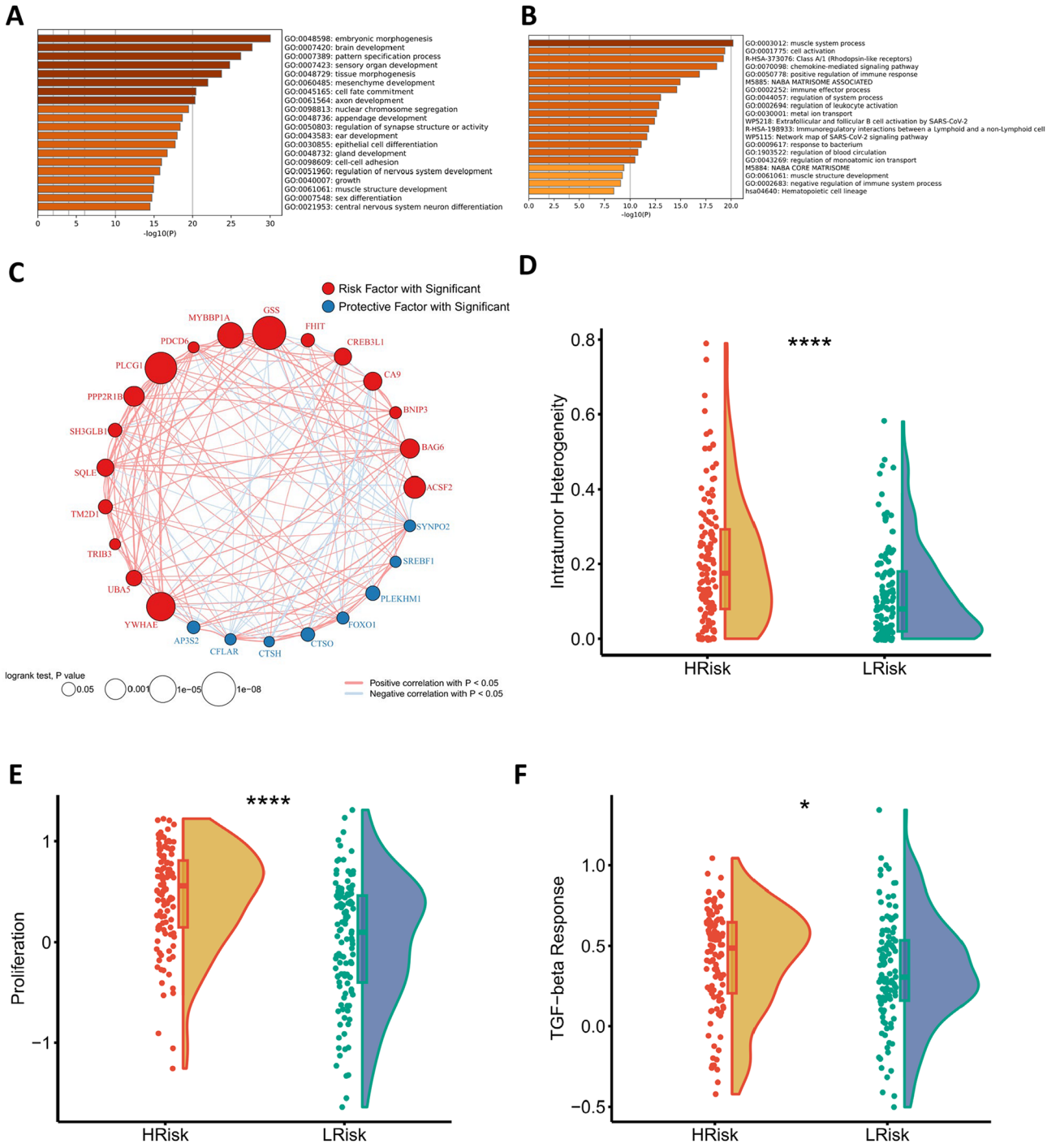

Fig. 6 Functional annotation of the CDSig in STS based on the TCGA database. **A** The enrichment analysis of upregulated genes in the high-CDS group. **B** The enrichment analysis of upregulated genes in the low-CDS group. **C** The prognostic value and correlations of 25 signature genes in STS. **D**–**F** The difference in Intratumor heterogeneity, proliferation, and TGF-beta response scores between two low and high CDSig risk groups. *HRisk* High risk; *LRisk* Low risk

immunotherapy compared to those with high CDS. To further explore the link between CDSig and drug sensitivity, we computed and compared the half-maximal inhibitory concentration (IC50) values for commonly used drugs, including Doxorubicin, Axitinib, Cisplatin, and Camptothecin, in the TCGA and TARGET cohorts. The results of the drug sensitivity comparison are depicted in Fig. 8E, F. We observed that the IC50 values of Doxorubicin, Axitinib, Cisplatin, and Camptothecin were higher in the high CDSig group compared to the low CDSig group in both datasets. These findings suggest

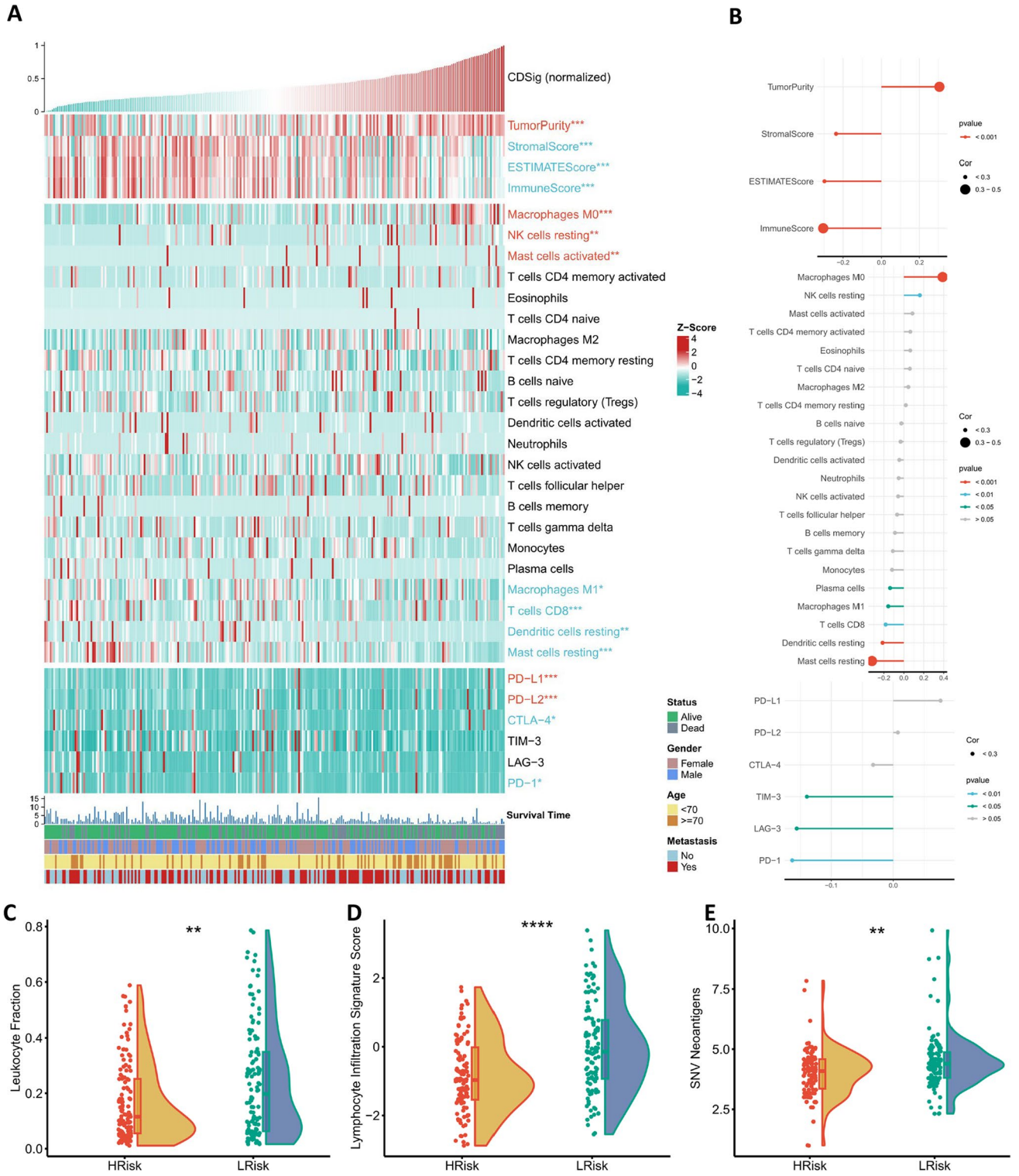

Fig. 7 Dissection of tumor immunity microenvironment of CDSig in STS based on the TCGA database. **A** The heatmap revealed the difference in the immune score, immune infiltrating cells, and immune checkpoint between distinct CDSig groups. **B** Correlations between the CDSig and immune score, immune infiltrating cells, and immune checkpoint using Spearman's analysis. **C** Box plot displaying the leukocyte fraction level between two CDSig groups. **D** Box plot displaying the lymphocyte infiltration signature score between two CDSig groups. **E** Box plot displaying the SNV Neoantigens score between two CDSig groups. *CDSig* cell death-related signatures; *HRisk* High risk; *LRisk* Low risk; *SNV* single nucleotide variation

Fig. 8 Efficacy of CDSig in predicting immunotherapy response and drug sensitivity based on the TCGA and TARGET database. **A** Contingency table between immunotherapy responses and CDSig groups based on the TIDE algorithm in the TCGA cohort. **B** Submap of immunotherapy responses (anti-PD-1 and anti-CTLA-4) and CDSig groups based on submap analysis in the TCGA cohort. **C** Contingency table between immunotherapy responses and CDSig groups based on the TIDE algorithm in the TARGET cohort. **D** Submap of immunotherapy responses (anti-PD-1 and anti-CTLA-4) and CDSig groups based on submap analysis in the TARGET cohort. **E** The boxplots of the comparison of IC50 of chemotherapy drugs between high- and low-CDS groups in the TCGA cohort. **F** The boxplots of the comparison of IC50 of chemotherapy drugs between high- and low-CDS groups in the TARGET cohort. **G** The description of the mode of action of compounds targeting corresponding molecular pathways based on the TCGA database. *HCDSig* High cell death-related signature group; *LCDSig* Low cell death-related signature group

that individuals with high CDS in STS may exhibit resistance to these drugs. Additionally, we utilized the Cmap database to identify 40 small-molecule drugs with potential therapeutic effects on STS based on the top 150 DEGs between the high and low CDSig groups in STS patients. The names and mechanisms of these small-molecule agents are presented in Fig. 8G.

3.8 Verification of the CDSig genes in STS

To further validate the robustness of our study, we selected the top 8 genes from the CDSig and assessed their expression in STS cells using RT-qPCR. The PCR results revealed substantial differential expression of these genes across various STS cell lines. Specifically, PLCG, BAG6, and SQLE exhibited elevated expression, while ACSF2, GSS, MYBBP1 A, PPP2R1B, and YWHAE displayed the opposite trend in distinct STS cell lines (Fig. 9). Thus, these CDSig genes demonstrated significant differences in STS cell lines, indirectly affirming the reliability and accuracy of previous analysis.

4 Discussion

STS is an infrequent tumor, characterized by a remarkable diversity in its pathological and histological types, which contributes to its significant heterogeneity. There are 19 histological types and more than 50 different subtypes, so there are large differences in individual curative effects in clinical treatment [26]. Recent efforts have focused on exploring the genomic and transcriptomic characteristics of STS in order to uncover its molecular profile and identify potential therapeutic targets. These endeavors have spurred the adoption of individualized treatment approaches for STS patients [23, 24]. Despite these insightful findings, the development of a comprehensive predictive model tailored for individualized diagnosis and treatment in STS patients remains challenging. PCD is recognized as a multifaceted form of cell death involving multiple mechanisms that resist characterization under a single form of demise [27]. A growing body of evidence emphasizes the fundamental role of PCD in various biological processes, linking it to the development and metastasis of malignancies for several decades [12]. Although STS has been associated with several PCD-related signatures, many studies predominantly focus on the significance of individual PCD patterns in STS prognosis. Therefore, our objective is to conduct a comprehensive analysis of 12 distinct PCD patterns in STS, utilizing machine learning algorithms to construct and validate the CDSig. Additionally, we aim to investigate the potential associations of CDSig with the tumor microenvironment, immunotherapy response, and drug sensitivity.

We constructed a novel CDSig by utilizing PCD-related genes gathered from prior studies and implementing a comprehensive framework entailing 10 machine learning algorithms. This CDSig comprises 25 genes that are associated with PCD. Remarkably, our signature exhibited superior predictive efficacy across diverse cohorts and outperformed existing prognostic models for STS. Furthermore, univariate and multivariate regression analyses provided further validation of the novel CDSig as an independent risk factor for STS. Additionally, we formulated a nomogram that integrates CDS and clinical characteristics, revealing its robust predictive capabilities for prognosis.

To validate our analytical findings, we performed RT-qPCR to assess the expression of PCD-related genes (PLCG1, BAG6, SQLE, ACSF2, GSS, MYBBP1 A, PPP2R1B, and YWHAE) in STS. The results unequivocally demonstrated aberrant expression of these genes in STS. Importantly, the dysregulation of these genes has been linked to tumor development. PLCG1 recognized as a multifunctional protein, has been associated with the growth and poor prognosis of IDH wild-type LGG, serving as a potential therapeutic target for patients with this condition [28]. BAG6, also known as Bat-3/Scythe, participates in various cellular processes, including apoptosis, gene regulation, and protein synthesis [29]. In colorectal cancer, GET4-induced cytoplasmic translocation of BAG6 regulates p53 acetylation to reduce p21 expression, thereby influencing cancer progression [30]. SQLE, a crucial molecule in cholesterol synthesis, is overexpressed in various malignancies such

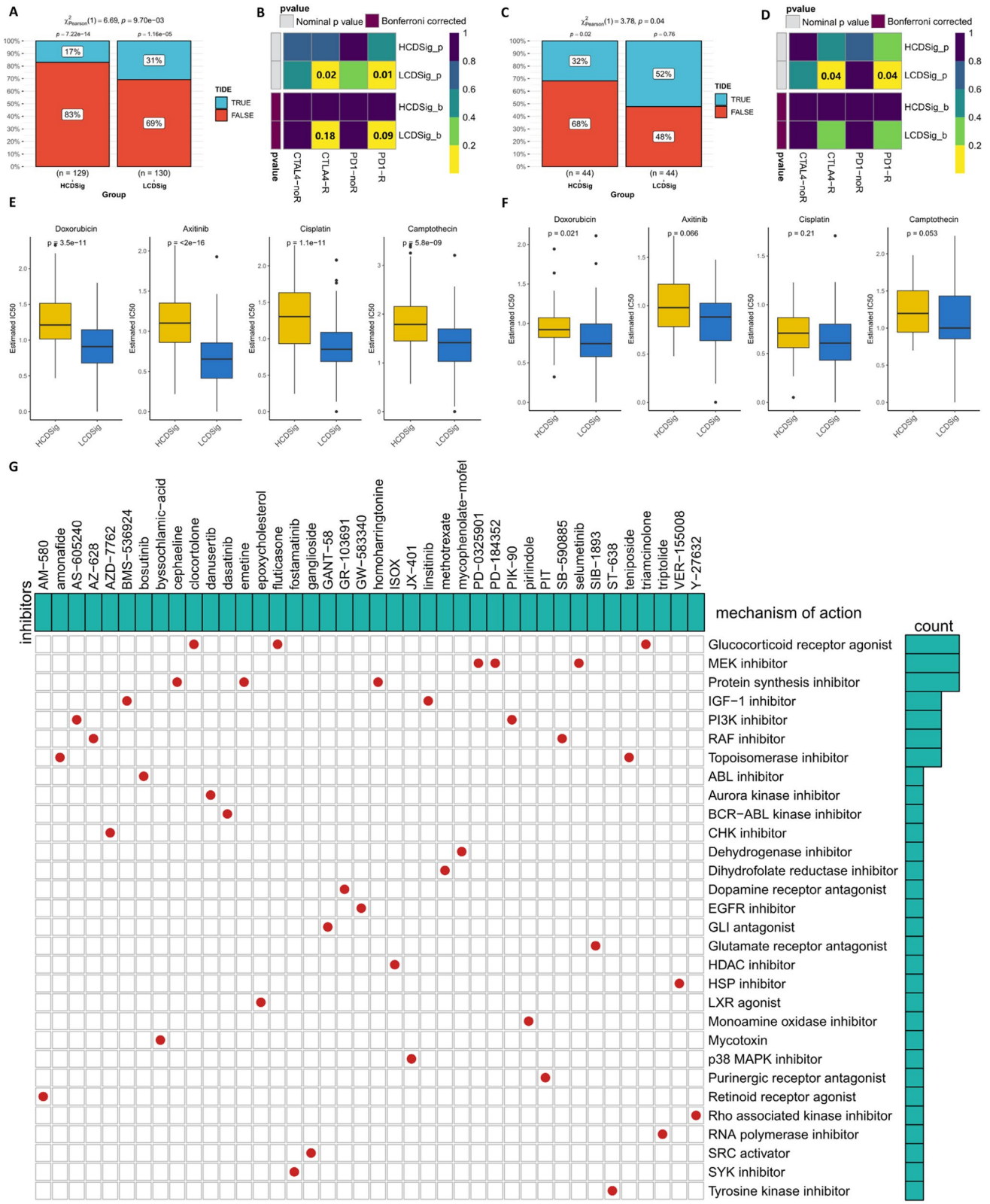

as breast cancer, colorectal cancer, lung squamous cell carcinoma, esophageal squamous cell carcinoma, and hepatocellular carcinoma [31–34]. Our study also revealed its overexpression in STS. ACSF2, identified as an essential molecule in cholesterol synthesis, demonstrated elevated expression in hepatocellular carcinoma tissues, indicating its potential

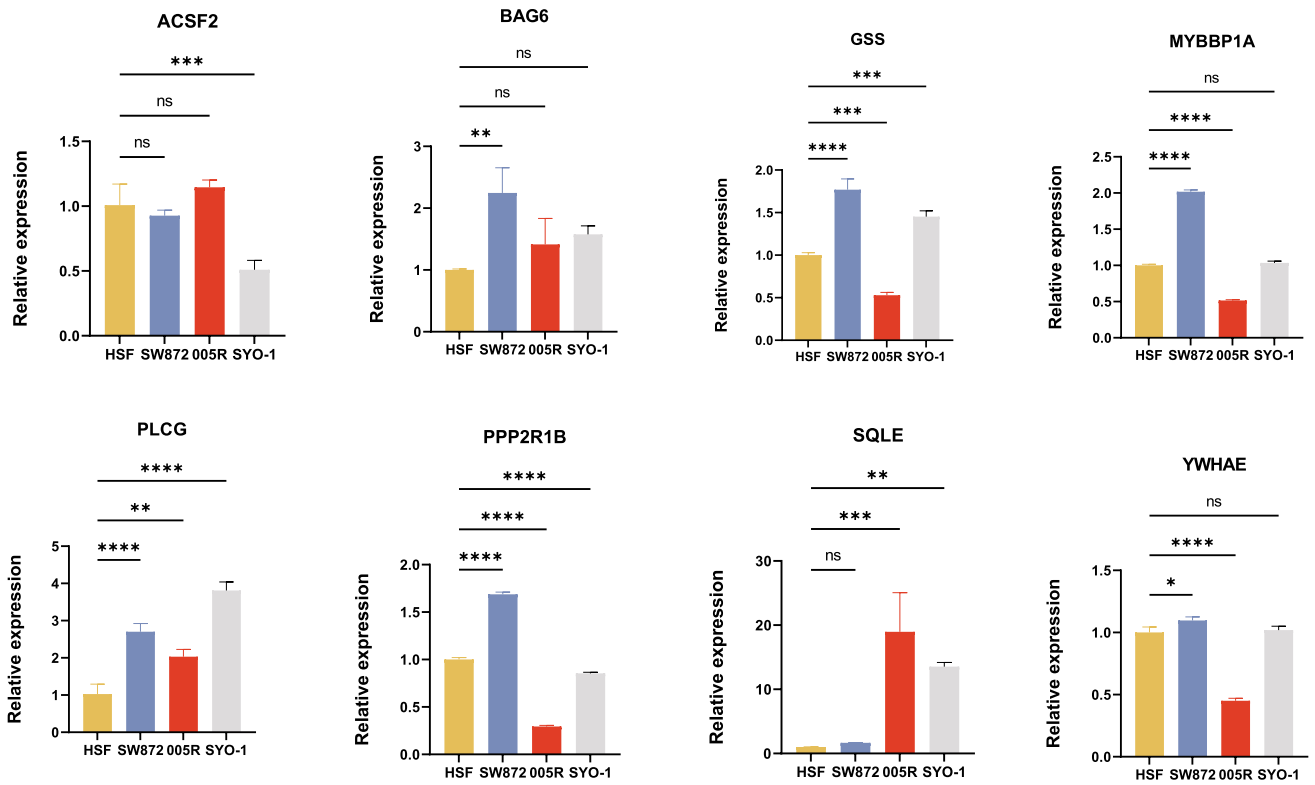

Fig. 9 The expression of several CDSig genes was confirmed by RT−qPCR in HSF and STS cell lines

involvement in disease progression [35]. Glutathione synthase (GSS), pivotal in catalyzing glutathione (GSH) synthesis, plays a role in protecting cancer cells from potential ferroptosis [36]. Previous research indicates that RRM2 can maintain intracellular GSH by safeguarding GSS from degradation [37]. MYB-binding protein 1a (MYBBP1 A) is a nucleolar transcriptional regulator whose role in solid tumors remains controversial. On the one hand, Akaogi K et al. demonstrated that MYBBP1 A functions as a tumor suppressor protein in breast cancer by enhancing anoikis [38]. On the other hand, MYBBP1 A promoted tumor cell proliferation in the early stage of head and neck squamous cell carcinoma (HNSCC), while its inactivation accelerated the migration and invasion of tumor cells in advanced tumors [39]. PPP2R1B, identified as a tumor suppressor, has mutations and alterations observed in various human cancers, including colon, lung, and cancer, and is associated with chemosensitivity [40–42]. Recent studies highlight the significant role of YWHAE in various tumors. For instance, it is overexpressed in renal cancer tissues and has been shown to promote abnormal proliferation of tumor cells in vitro [43]. Although we have confirmed that these genes do have differential expression in STS, their roles in STS and their relationship with CDSig still deserve further exploration in the future.

The robustness of tumor cells, marked by their ability to evade immune responses and resist drug interference, is significantly influenced by the tumor microenvironment [44]. Theoretically, higher programmed cell death (PCD) scores in a tumor may lead to reduced expression of immune checkpoints and diminished infiltration of anti-tumor immune cells, indicative of an impaired overall immune function [45, 46]. In line with this theoretical framework, our observations reveal that the low CDS group exhibits elevated immune scores, stromal scores, and increased infiltration of various immune cell types compared to the high CDS group. Specifically, there is a negative correlation between M1 macrophages and CDS, while M0 macrophages show a positive correlation. Notably, M0 macrophages are considered quiescent and possess the ability to differentiate into M1 and M2 phenotypes. M1 macrophages predominantly exert pro-inflammatory and anti-tumor functions, while M2 macrophages are primarily involved in anti-inflammatory and pro-tumor responses [47]. This observed correlation may contribute to the improved prognosis observed in STS patients within the low CDS group. Generally, PCD activity appears to align with an anti-inflammatory profile, consistent with our findings. Previous studies have highlighted that an increased abundance of M1 macrophages in the STS microenvironment is associated with a more favorable prognosis, whereas the enrichment of M2 macrophages is linked to a poorer prognosis [48]. Therefore, strategies aimed at promoting the activation of M0 macrophages into M1 macrophages may represent a viable approach to mitigating inflammation and enhancing the prognosis of STS.

Currently, cancer treatment is showing great promise in the field of immunological therapy. This approach aims to enhance the immune system's response and stimulate cancer cell death. Techniques in this area include immune checkpoint inhibitors, tumor antigen vaccines, CAR-T cell therapy, and immunotherapy involving immune cells [49]. However, the effectiveness of immunotherapy varies among patients, with only a subset experiencing substantial benefits, while others show limited or no response. Therefore, it is crucial to determine the responsiveness of STS patients to immunotherapy, as this information greatly influences their clinical management [50]. In this study, we evaluated the predictive capability of CDSig for immunological therapeutic response. Using the TIDE algorithm, we observed that STS patients with lower CDSig levels demonstrated a more promising response to immune checkpoint blockade (ICB). Consistent with these findings, the submap results in both TCGA and TARGET cohorts indicated that patients with low CDSig were more sensitive to treatments involving anti-CTLA4 and anti-PD-1 agents. Thus, our findings have significant implications for the prospective identification of patients likely to respond favorably to immunotherapy.

In addition, the utilization of chemotherapy and targeted gene therapy provides several advantages in improving and prolonging the survival of individuals with STS. Therefore, predicting the therapeutic response of STS to chemotherapeutic agents and molecularly targeted antineoplastic agents is of great importance. Our investigation revealed that patients in the low CDSig group exhibited lower IC50 values for doxorubicin, axitinib, cisplatin, and camptothecin compared to those in the high CDSig group. This finding may explain the poorer prognosis of patients with high CDSig levels, as they demonstrated increased resistance to these chemotherapeutic agents. Furthermore, our exploration of public datasets enabled us to identify representative potential drugs and elucidate their associated mechanisms, providing insights that could effectively mitigate drug resistance in high-risk STS patients. Hence, this CDSig demonstrates a close association with chemotherapy, facilitating the implementation of personalized drug therapy strategies for the STS cohort.

While the CDSig signature demonstrates substantial clinical significance in STS, some limitations in this study need to be issued. Firstly, all datasets utilized are derived from single-center, retrospective studies. Therefore, the prognostic value of the novel CDSig needs to be further validated in prospective, multi-center cohorts. Moreover, the limited availability of certain clinical and molecular data in public repositories restricted the inclusion of key clinical factors. For instance, the GEO dataset is deficient in-patient clinical information, including age, gender, and the presence of metastasis, precluding the creation of a nomogram based on this dataset. Furthermore, the scarcity of chemotherapy-related clinical data in the TCGA and TARGET databases hinders our ability to explore the effects of chemotherapy on cellular patterns and to refine the stratification of STS into more specific subtypes. The precise mechanisms underlying the interaction between the identified CDSig and the tumor immune microenvironment remain unclear and merit further investigation, which may facilitate the development of novel therapeutic targets and translational applications. Lastly, although we have conducted a preliminary exploration of the differences in immunotherapy responses among patients in different CDSig groups, there is a pressing need for larger immunotherapy cohorts of STS patients to thoroughly validate the predictive utility of CDSig in assessing responses to immunotherapy.

5 Conclusion

In conclusion, the novel CDSig proposed in this study is a practical prognostic indicator for STS, crucial for the clinical prognosis assessment and individualized immune therapy and chemotherapy of STS.

Acknowledgements Thank all members of the TCGA and GEO database for providing a good platform for researchers.

Author contributions CT and ZL contributed to the conception and made final approval of the version, BL performed the study concept and design and wrote the manuscript. SH performed data analysis. CF, HW, ZX, and CL helped with data analysis. All authors contributed to the manuscript revision read, and approved the submitted version.

Funding This work was supported by the National Natural Science Foundation of China (82272664, 82172500), the Science and Technology Innovation Program of Hunan Province (2023RC3085), Hunan Provincial Health High-Level Talent Scientific Research Project (R2023054), Key Project of Scientific Research of the Education Department of Hunan Province (24 A0008), Hunan Provincial Administration of Traditional Chinese Medicine Project (D2022117), the Natural Science Foundation of Hunan Province, China (2023 JJ40822), the Health Research Project of Hunan Provincial Health Commission (202105012224), The Fundamental Research Funds for the Central Universities of Central South University (2024ZZTS0174) and the Scientific Research Program of Hunan Provincial Health Commission (B202304077077).

Availability of data and material The original contributions presented in the study are publicly available. The names of the database and accession number(s) can be found in the article.

Declarations

Ethics approval and consent to participate Not applicable.

Consent for publication Not applicable.

Competing Interests The authors declare no competing interests.

References

1. Karakousis CP, Perez RP. Soft tissue sarcomas in adults. CA Cancer J Clin. 1994;44(4):200–10.
2. Qi L, Ren X, Liu Z, Li S, Zhang W, Chen R, et al. Predictors and survival of patients with osteosarcoma after limb salvage versus amputation: a population-based analysis with propensity score matching. World J Surg. 2020;44(7):2201–10.
3. Kallen ME, Hornick JL. The 2020 WHO classification: what's new in soft tissue tumor pathology? Am J Surg Pathol. 2021;45(1):e1–23.
4. Wang S, Wang H, Feng C, Li C, Li Z, He J, et al. The regulatory role and therapeutic application of pyroptosis in musculoskeletal diseases. Cell Death Discov. 2022;8(1):492.
5. Gronchi A, Colombo C, Raut CP. Surgical management of localized soft tissue tumors. Cancer. 2014;120(17):2638–48.
6. Rydholm A. Improving the management of soft tissue sarcoma. Diagnosis and treatment should be given in specialist centres. Bmj. 1998;317(7151):93–4.
7. Frezza AM, Stacchiotti S, Gronchi A. Systemic treatment in advanced soft tissue sarcoma: what is standard, what is new. BMC Med. 2017;15(1):109.
8. Dangoor A, Seddon B, Gerrand C, Grimer R, Whelan J, Judson I. UK guidelines for the management of soft tissue sarcomas. Clin Sarcoma Res. 2016;6:20.
9. Meyer M, Seetharam M. First-line therapy for metastatic soft tissue sarcoma. Curr Treat Options Oncol. 2019;20(1):6.
10. Tang D, Kang R, Berghe TV, Vandenabeele P, Kroemer G. The molecular machinery of regulated cell death. Cell Res. 2019;29(5):347–64.
11. Chen X, Zeh HJ, Kang R, Kroemer G, Tang D. Cell death in pancreatic cancer: from pathogenesis to therapy. Nat Rev Gastroenterol Hepatol. 2021;18(11):804–23.
12. Su Z, Yang Z, Xu Y, Chen Y, Yu Q. Apoptosis, autophagy, necroptosis, and cancer metastasis. Mol Cancer. 2015;14:48.
13. Han Y, Li B, Yan D, Zhou D, Yuan X, Zhao W, et al. Combining multiple cell death pathway-related risk scores to develop neuroblastoma cell death signature. J Cancer Res Clin Oncol. 2023;149(9):6513-6526.
14. Liu Z, Liu B, Feng C, Li C, Wang H, Zhang H, et al. Molecular characterization of immunogenic cell death indicates prognosis and tumor microenvironment infiltration in osteosarcoma. Front Immunol. 2022;13:1071636.
15. Zou Y, Xie J, Zheng S, Liu W, Tang Y, Tian W, et al. Leveraging diverse cell-death patterns to predict the prognosis and drug sensitivity of triple-negative breast cancer patients after surgery. Int J Surg. 2022;107: 106936.
16. Liu Z, Xu H, Weng S, Guo C, Dang Q, Zhang Y, et al. Machine learning algorithm-generated and multi-center validated melanoma prognostic signature with inspiration for treatment management. Cancer Immunol Immunother. 2023;72(3):599–615.
17. Thorsson V, Gibbs DL, Brown SD, Wolf D, Bortone DS, Ou Yang TH, et al. The immune landscape of cancer. Immunity. 2018;48(4):812–30.
18. Yoshihara K, Shahmoradgoli M, Martínez E, Vegesna R, Kim H, Torres-Garcia W, et al. Inferring tumour purity and stromal and immune cell admixture from expression data. Nat Commun. 2013;4:2612.
19. Newman AM, Liu CL, Green MR, Gentles AJ, Feng W, Xu Y, et al. Robust enumeration of cell subsets from tissue expression profiles. Nat Methods. 2015;12(5):453–7.
20. Zhang N, Zhang H, Wu W, Zhou R, Li S, Wang Z, et al. Machine learning-based identification of tumor-infiltrating immune cell-associated lncRNAs for improving outcomes and immunotherapy responses in patients with low-grade glioma. Theranostics. 2022;12(13):5931–48.
21. Charoentong P, Finotello F, Angelova M, Mayer C, Efremova M, Rieder D, et al. Pan-cancer immunogenomic analyses reveal genotype-immunophenotype relationships and predictors of response to checkpoint blockade. Cell Rep. 2017;18(1):248–62.
22. Liu B, Pang K, Feng C, Liu Z, Li C, Zhang H, et al. Comprehensive analysis of a novel cuproptosis-related lncRNA signature associated with prognosis and tumor matrix features to predict immunotherapy in soft tissue carcinoma. Front Genet. 2022;13:1063057.
23. Liu B, Liu Z, Feng C, Tu C. A necroptosis-related lncRNA signature predicts prognosis and indicates the immune microenvironment in soft tissue sarcomas. Front Genet. 2022;13: 899545.
24. Liu B, He S, Li C, Feng C, Wang H, Zhang H, et al. Integration analysis based on fatty acid metabolism robustly predicts prognosis, dissecting immunity microenvironment and aiding immunotherapy for soft tissue sarcoma. Front Genet. 2023;14:1161791.
25. Tu C, Liu B, Li C, Feng C, Wang H, Zhang H, et al. Integrative analysis of TROAP with molecular features, carcinogenesis, and related immune and pharmacogenomic characteristics in soft tissue sarcoma. MedComm. 2020;4(5): e369.

26. von Mehren M, Kane JM, Bui MM, Choy E, Connelly M, Dry S, et al. NCCN guidelines insights: soft tissue sarcoma, version 1.2021. J Natl Compr Canc Netw. 2020;18(12):1604–12.
27. Malireddi RKS, Kesavardhana S, Kanneganti TD. ZBP1 and TAK1: master regulators of NLRP3 Inflammasome/Pyroptosis, apoptosis, and necroptosis (PAN-optosis). Front Cell Infect Microbiol. 2019;9:406.
28. Li T, Yang Z, Li H, Zhu J, Wang Y, Tang Q, et al. Phospholipase Cγ1 (PLCG1) overexpression is associated with tumor growth and poor survival in IDH wild-type lower-grade gliomas in adult patients. Lab Invest. 2022;102(2):143–53.
29. Binici J, Koch J. BAG-6, a jack of all trades in health and disease. Cell Mol Life Sci. 2014;71(10):1829–37.
30. Koike K, Masuda T, Sato K, Fujii A, Wakiyama H, Tobo T, et al. GET4 is a novel driver gene in colorectal cancer that regulates the localization of BAG6, a nucleocytoplasmic shuttling protein. Cancer Sci. 2022;113(1):156–69.
31. Helms MW, Kemming D, Pospisil H, Vogt U, Buerger H, Korsching E, et al. Squalene epoxidase, located on chromosome 8q24.1, is upregulated in 8q+ breast cancer and indicates poor clinical outcome in stage I and II disease. Br J Cancer. 2008;99(5):774–80.
32. Kim JH, Kim CN, Kang DW. Squalene epoxidase correlates E-cadherin expression and overall survival in colorectal cancer patients: the impact on prognosis and correlation to clinicopathologic features. J Clin Med. 2019;8(5):632.
33. Ge H, Zhao Y, Shi X, Tan Z, Chi X, He M, et al. Squalene epoxidase promotes the proliferation and metastasis of lung squamous cell carcinoma cells though extracellular signal-regulated kinase signaling. Thorac Cancer. 2019;10(3):428–36.
34. Qin Y, Zhang Y, Tang Q, Jin L, Chen Y. SQLE induces epithelial-to-mesenchymal transition by regulating of miR-133b in esophageal squamous cell carcinoma. Acta Biochim Biophys Sin (Shanghai). 2017;49(2):138–48.
35. Zhao Z, Liu M, Xu Z, Cai Y, Peng B, Liang Q, et al. Identification of ACSF gene family as therapeutic targets and immune-associated biomarkers in hepatocellular carcinoma. Aging (Albany NY). 2022;14(19):7926–40.
36. Chen X, Li J, Kang R, Klionsky DJ, Tang D. Ferroptosis: machinery and regulation. Autophagy. 2021;17(9):2054–81.
37. Yang Y, Lin J, Guo S, Xue X, Wang Y, Qiu S, et al. RRM2 protects against ferroptosis and is a tumor biomarker for liver cancer. Cancer Cell Int. 2020;20(1):587.
38. Akaogi K, Ono W, Hayashi Y, Kishimoto H, Yanagisawa J. MYBBP1A suppresses breast cancer tumorigenesis by enhancing the p53 dependent anoikis. BMC Cancer. 2013;13:65.
39. Acuña Sanhueza GA, Faller L, George B, Koffler J, Misetic V, Flechtenmacher C, et al. Opposing function of MYBBP1A in proliferation and migration of head and neck squamous cell carcinoma cells. BMC Cancer. 2012;12:72.
40. Wang SS, Esplin ED, Li JL, Huang L, Gazdar A, Minna J, et al. Alterations of the PPP2R1B gene in human lung and colon cancer. Science. 1998;282(5387):284–7.
41. Tamaki M, Goi T, Hirono Y, Katayama K, Yamaguchi A. PPP2R1B gene alterations inhibit interaction of PP2A-Abeta and PP2A-C proteins in colorectal cancers. Oncol Rep. 2004;11(3):655–9.
42. Yeh LS, Hsieh YY, Chang JG, Chang WW, Chang CC, Tsai FJ. Mutation analysis of the tumor suppressor gene PPP2R1B in human cervical cancer. Int J Gynecol Cancer. 2007;17(4):868–71.
43. Liang S, Xu Y, Shen G, Liu Q, Zhao X, Xu Z, et al. Quantitative protein expression profiling of 14-3-3 isoforms in human renal carcinoma shows 14-3-3 epsilon is involved in limitedly increasing renal cell proliferation. Electrophoresis. 2009;30(23):4152–62.
44. Zou Y, Zheng S, Deng X, Yang A, Xie X, Tang H, et al. The role of circular RNA CDR1as/ciRS-7 in regulating tumor microenvironment: a pan-cancer analysis. Biomolecules. 2019. 9(9):429.
45. Zou Y, Zou X, Zheng S, Tang H, Zhang L, Liu P, et al. Efficacy and predictive factors of immune checkpoint inhibitors in metastatic breast cancer: a systematic review and meta-analysis. Ther Adv Med Oncol. 2020;12:1758835920940928.
46. Zou Y, Hu X, Zheng S, Yang A, Li X, Tang H, et al. Discordance of immunotherapy response predictive biomarkers between primary lesions and paired metastases in tumours: a systematic review and meta-analysis. EBioMedicine. 2021;63: 103137.
47. Mohapatra S, Pioppini C, Ozpolat B, Calin GA. Non-coding RNAs regulation of macrophage polarization in cancer. Mol Cancer. 2021;20(1):24.
48. Lv M, He F, Guo J, Zheng Z, Wang W, Xie J. Identification of hub genes correlated with tumor-associated M1-like macrophage infiltration in soft tissue sarcomas. Front Genet. 2022;13: 999966.
49. Lin A, Wei T, Meng H, Luo P, Zhang J. Role of the dynamic tumor microenvironment in controversies regarding immune checkpoint inhibitors for the treatment of non-small cell lung cancer (NSCLC) with EGFR mutations. Mol Cancer. 2019;18(1):139.
50. Braun DA, Burke KP, Van Allen EM. Genomic approaches to understanding response and resistance to immunotherapy. Clin Cancer Res. 2016;22(23):5642–50.